Hydrothermal Synthesis of Mn_3O_4/CoS_2 as a Promising Photocatalytic Material for Boosting Visible-Light Photocatalytic Hydrogen Production

Jing Xu,* Ye Liu, Xuanhao Li, and Yanru Li

Photocatalytic hydrogen evolution has received extensive attention for energy conversion and storage of clean energy. Herein, the composite catalyst Mn_3O_4/CoS_2 is successfully prepared by a hydrothermal method. Photocatalytic hydrogen evolution experiments are conducted by adjusting the amount of Mn_3O_4. The results show that the composite photocatalyst Mn_3O_4/CoS_2 has higher photocatalytic hydrogen evolution performance. The hydrogen production of the 50 mg Mn_3O_4/CoS_2 composite catalyst at 5 h is 14.95 times and 1.60 times that of pure Mn_3O_4 and CoS_2, respectively, indicating that the 50 mg Mn_3O_4/CoS_2 composite catalyst has good photocatalytic stability. In addition, the structure, morphology, and composition of the prepared catalysts are characterized by scanning electron microcopy (SEM), transmission electron microscopy (TEM), X-ray diffraction (XRD), X-ray photoelectron spectroscopy (XPS), Brunauer–Emmett–Teller (BET), electrochemical and PL techniques. Compared with Mn_3O_4 and CoS_2, the photocatalytic response of the 50 mg Mn_3O_4/CoS_2 composite catalyst is significantly enhanced, the current density is increased, the fluorescence quenching efficiency is accelerated, and the pore volume and pore size are increased. Therefore, the composite catalyst can accelerate the separation and transfer of photogenerated electrons and holes and improve the photocatalytic efficiency.

1. Introduction

Hydrogen (H_2) is a renewable energy source, and it has been widely regarded for its advantages of nonpollutant emission and high energy density.[1–3] Solar energy is a kind of inexhaustible energy, which also attracts attention. In the past, semiconductor photocatalysts have been used to convert solar energy into chemical energy, through solar energy to produce hydrogen.[2,4,5] Because this technology neither depends on fossil fuels nor emits pollutants, it is considered to be an attractive and promising way to solve global energy problems.[6] However, the development of highly efficient and inexpensive photocatalysts for photocatalytic hydrogen evolution remains a great challenge.[7] Initially, it was the first water splitting system TiO_2 reported by Fujishima and Honda in 1972,[8] and since then, as photocatalysts, many materials have made great efforts in photocatalytic hydrogen evolution. Among all kinds of photocatalytic materials, Mn_3O_4 is an environmentally friendly material because of its abundant resources, affordable price, and no pollution to the environment.[9] Furthermore, manganese oxides have been extensively studied due to their novel structures and excellent physical and chemical applications.[10] Among these manganese oxides, Mn_3O_4 is an interesting material for researchers because of its remarkable surface area and unique electronic structure at nanoscale, which is suitable for wide applications, such as its use as a thermochemical energy storage material[11] and many applications in the field of biomedicine.[12] Mn_3O_4 is a stable oxide with spinel structure. It also has catalytic and electrochemical properties.[13,14] For example, it is used for electrochemical water splitting to produce hydrogen,[15] photodegradation of organic pollutants in water,[16] preparation of photoelectrochemical oxygen evolution reaction,[17] using Mn_3O_4 as cocatalyst, etc. In this study, we choose Mn_3O_4 as a photocatalyst for hydrogen production from water decomposition. The improper optical bandgap and easy recombination of photogenerated carriers lead to unfavorable photocatalytic performance, so it is necessary to modify Mn_3O_4. Recently, transition metal sulfides (Ni, Co, Fe, and Mn) have attracted wide attention due to their abundance in the earth and environmental friendliness.[18–22] Among them, cobalt sulfide compounds have great attraction in

Prof. J. Xu, Y. Liu, X. Li, Y. Li
School of Chemistry and Chemical Engineering
North Minzu University
Yinchuan 750021, P. R. China
E-mail: xujing@nmu.edu.cn, wgyxj2000@163.com

Prof. J. Xu
State Key Laboratory of High-efficiency Utilization of Coal and Green Chemical Engineering
Ningxia University
Yinchuan 750021, P. R. China

Prof. J. Xu
Ningxia Key Laboratory of Solar Chemical Conversion Technology
North Minzu University
Yinchuan 750021, P. R. China

Prof. J. Xu
Key Laboratory for Chemical Engineering and Technology
State Ethnic Affairs Commission
North Minzu University
Yinchuan 750021, P. R. China

The ORCID identification number(s) for the author(s) of this article can be found under https://doi.org/10.1002/pssa.202100025.

thermal stability, energy storage, and conductivity.[23] There are cobalt sulfide compounds with different chemical formulas (Co_3S_4, CoS, CoS_2, and Co_9S_8) in lithium ion batteries, electrocatalysis,[24] degradation of organic matter,[25] and dye-sensitized solar cells (DSSCs) to construct cobalt sulfide/carbon hybrid materials doped with heteroatoms.[26] They have all been studied. Among them, CoS_2 is considered to be a good catalyst because of its high electrical conductivity and high activity.[27,28] Here, we report a novel composite photocatalyst, Mn_3O_4/CoS_2, which has not been reported before. The composite catalyst Mn_3O_4/CoS_2 was successfully prepared by a hydrothermal method. In this experiment, the amount of Mn_3O_4 added was investigated in detail; compared with pure Mn_3O_4 and pure Mn_3O_4, the composite catalyst 50 mg Mn_3O_4/CoS_2 effectively inhibited the photoelectron–hole pair recombination and exposed more active sites, thereby exhibiting good photocatalytic hydrogen evolution activity and good photocatalytic stability. Therefore, the obtained Mn_3O_4/CoS_2 composite material has a photocatalytic application prospect and is a low-cost noble metal–free catalytic material.

2. Experimental Section

2.1. Materials

All materials were analytical grade and there was no purification in this work: manganese acetate tetrahydrate ($(CH_3COO)_2 \cdot 4H_2O$), sodium hydroxide (NaOH), cobaltous nitrate hexahydrate ($Co(NO_3)_2 \cdot 6H_2O$), sodium thiosulfate pentahydrate ($Na_2S_2O_3 \cdot 5H_2O$), Eosin Y (EY, $C_{20}H_6Br_4Na_2O_5$), triethanolamine (TEOA), polyvinyl pyrrolidone (PVP), and deionized water was prepared by an ultrapure water machine.

2.2. Catalyst

2.2.1. Synthesis of Mn₃O₄ Photocatalysts

A total of 0.742 g manganese acetate tetrahydrate (Mn(CH_3COO)$_2 \cdot 4H_2O$) was accurately weighed and poured into a beaker filled with 60 mL deionized water, and then stirred on a magnetic stirrer. A total of 0.4 g NaOH was taken and slowly poured into the beaker to form a mixed solution. After mixing for 1 h, the homogeneous solution was poured into a 100 mL autoclave. Then the autoclave was put into the oven at 180 °C for 11 h by hydrothermal treatment. After, the solution was cooled to room temperature and filtered. Finally, the product was dried in a drying box for 4 h, and the product Mn_3O_4 was obtained (**Scheme 1**).

2.2.2. Preparation of Composite Photocatalyst Mn₃O₄/CoS₂

The composite catalyst Mn_3O_4/CoS_2 was synthesized by the second step hydrothermal method. In the experiment, the aforementioned prepared 20 mg Mn_3O_4 was weighed and stirred in a beaker containing 60 mL deionized water. Then, the following raw materials were weighed: 5 mmol cobalt nitrate hexahydrate ($Co(NO_3)_2 \cdot 6H_2O$), 1.2409 g sodium thiosulfate pentahydrate ($Na_2S_2O_3 \cdot 5H_2O$), and 500 mg PVP. These three chemicals were added into the stirring solution, respectively. The mixed solution was stirred for 2 h and transferred to a 100 mL autoclave. After treatment at 160 °C for 24 h, the solution was filtered, washed, and dried at room temperature. Finally, the Mn_3O_4/CoS_2 composite catalyst was prepared. CoS_2 was obtained by the same method without adding Mn_3O_4 (Scheme 1).

2.3. Characterization

X-ray diffraction (XRD) was detected with a Rigaku RINT-2000 to analyze the crystalline structure of the studied photocatalyst using Cu Kα radiation. The chemical valence and chemical components were performed by X-ray photoelectron spectroscopy (XPS) using ultrahigh vacuum VG ESCALAB 250 electron spectrometers. The morphology of the as-prepared materials was obtained by scanning electron microscopy (SEM, Japan JEOL, JSM-7500 F) operated at 20.0 kV voltage. The photoluminescence spectrum (PL) of the materials was investigated by a FLUOROMAX-4 spectrophotometer (HORIBA Scientific, France). The physical adsorption values of the catalyst were obtained at 77 K with an ASAP 2020 M instrument. The UV–vis diffuse-reflectance spectrum was obtained by a UV–vis spectrometer (UV-2500, SHIMADZU).

2.4. H₂ Evolution Experiment

Photocatalytic hydrogen evolution was conducted on a Perfect Light (PCX50B, $\lambda \geq 420$ nm) equipped with a magnetic stirring device. The light source was a 5 W LED lamp. In this program, the 10 mg catalyst powders were placed in 30 mL triethanolamine solution (TEOA, 10%, pH = 10). After mixing evenly, 20 mg EY was added to the solution. Then, the mixture was uniformly dispersed by magnetic stirring. The process described earlier was measured in a 65 ml quartz bottle. Before the light experiment, nitrogen needed to be injected into the quartz bottle to remove oxygen from the bottle. The hydrogen production
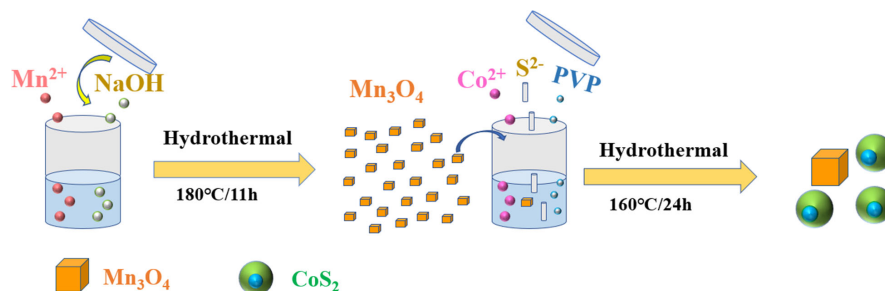
Scheme 1. Synthesis process diagram of Mn_3O_4/CoS_2 photocatalyst.

amount was obtained by gas chromatography (SP-2100, 13X column, TCD, N_2 carrier).

2.5. Photoelectrochemical Experiments

Electrochemical experiments were conducted by electrochemical instruments (CHI 660E, Shanghai Chen Hua Instrument Company). A Pt electrode was used as the counter electrode, and a saturated calomel electrode (SCE) as the reference electrode, and the working electrode was obtained on indium tin oxide (ITO) glass. The ITO was washed with absolute ethanol and then the ITO was naturally dried. 12 mg sample powder was placed in absolute ethanol and dispersed by sonication until the absolute ethanol evaporated and became a viscous liquid at room temperature. Subsequently, the viscous liquid was uniformly coated on the cleaned ITO by a pipette. The obtained working electrode was dried at room temperature. The supporting electrolyte was 0.2 M Na_2SO_4 aqueous solution. The sample area of the obtained working electrode was $\approx$1 cm^2. The light source was a 300 W xenon lamp (CEL-HXF300) with a 420 nm UV cut-off filter.

3. Results and Discussion

3.1. SEM and TEM Analysis

The morphologies of Mn_3O_4, CoS_2, and 50 mg Mn_3O_4/CoS_2 were observed by scanning electron microscopy (SEM, FESEM), transmission electron microscope (TEM, HRTEM). **Figure 1**a clearly shows that the prepared Mn_3O_4 displays a particle size of $\approx$100 nm. The morphology of CoS_2 and 50 Mg Mn_3O_4/CoS_2 composites was basically the same; the large spherical particles were covered by a few small spherical particles (Figure 1b,c). In the composite catalyst, the characteristic structure of Mn_3O_4 may not be observed because of the small amount of Mn_3O_4 added.[29] It may also be that the morphology of Mn_3O_4 is consistent with the larger spherical morphology of CoS_2, which makes it difficult to distinguish. Figure 1d shows a transmission electron microscopy (TEM) image of a composite sample. The light gray sheet-like structure in the figure is CoS_2, that is, the area marked by the red line, and the black circular sheet on the light gray line is Mn_3O_4, which is the area marked by yellow. The high-resolution transmission of the composite catalyst is shown in Figure 1e. The lattice spacing of CoS_2 is 0.28 nm, which
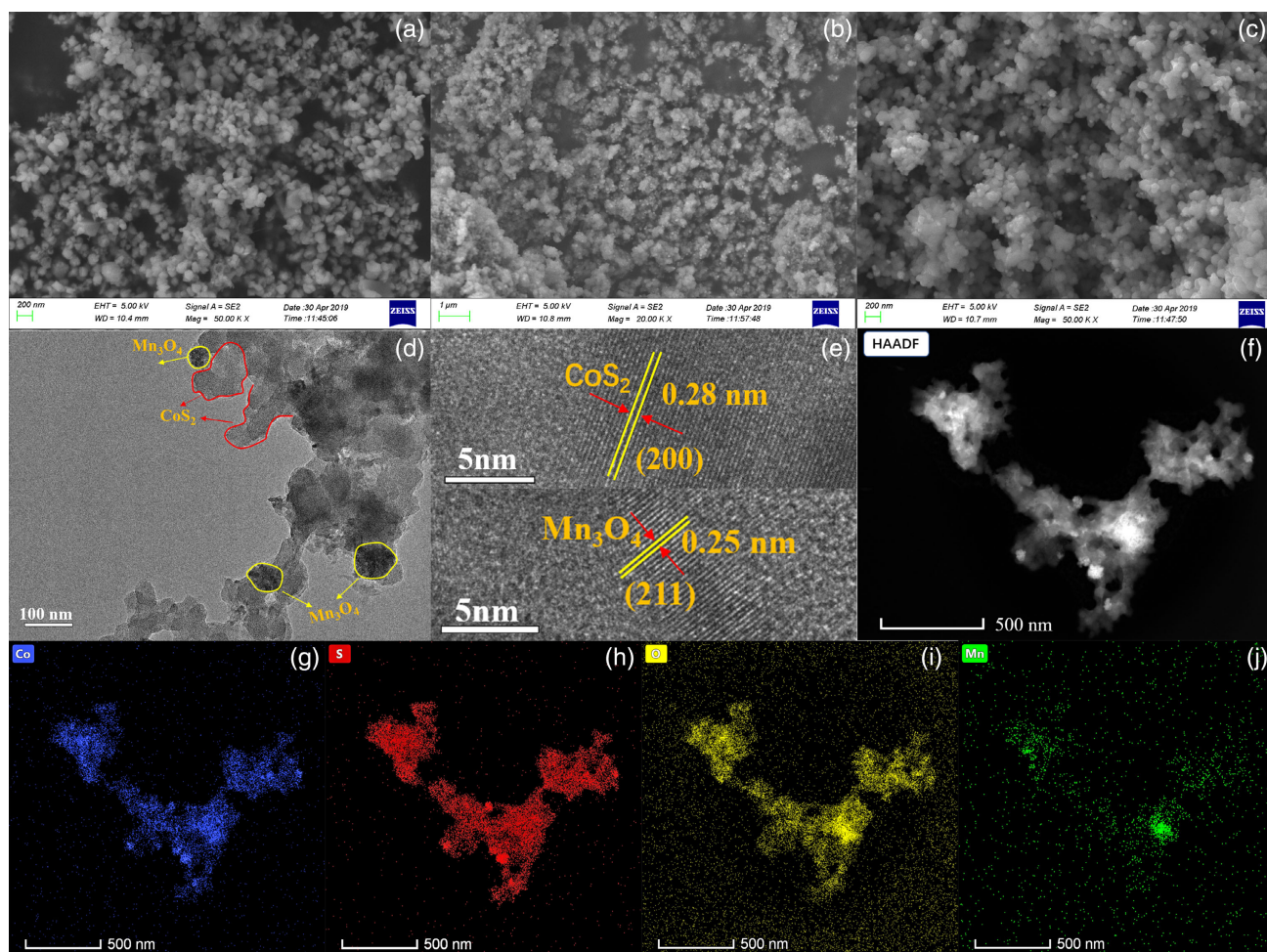

Figure 1. SEM images of a) Mn_3O_4, b) CoS_2, and c) 50 mg Mn_3O_4/CoS_2 samples. d) TEM images, e) HRTEM images, and f) elemental mapping micrographs of 50 mg Mn_3O_4/CoS_2 samples, showing the presence of g) Co, h) S, i) O, and j) Mn elements.

is consistent with the (200) crystal plane of CoS_2. The lattice spacing of Mn_3O_4 is 0.25 nm, which corresponds to the (211) crystal plane of Mn_3O_4. To understand the distribution uniformity of each element in the composite sample, the elemental mapping micrographs of the composite catalyst are shown in Figure 1g–j, and there are four elements Mn, O, S, and Co, and each element's distribution is relatively uniform. The content of the Mn element is small, which is also consistent with the SEM.

3.2. Phase Structure Analysis (XRD)

The phase structure of the prepared materials was studied by XRD, as shown in **Figure 2**. The Mn_3O_4 catalyst has several main diffraction peaks. At $2\theta = 18.00°$, $28.88°$, $31.02°$, $32.32°$, $36.08°$, $37.98°$, $44.44°$, $50.70°$, $58.51°$, $59.84°$, and $64.65°$, which can be well indexed to (101), (112), (200), (103), (211), (004), (220), (105), (321), (224), and (400) crystal faces of Mn_3O_4 (JCPDS#24-0734), respectively. The 2θ of CoS_2 samples is $27.8°$, $32.3°$, $36.2°$, $39.8°$, $46.3°$, and $54.9°$, the diffraction peaks of which match well with (111), (200), (210), (211), (220), and (311) crystal planes of CoS_2 (JCPDS 41-1471), respectively. It can be seen that the measured diffraction peaks of the pure catalyst Mn_3O_4 and pure catalyst CoS_2 correspond to those on standard cards. In the composite catalyst 50 mg Mn_3O_4/CoS_2, there are fewer characteristic peaks of Mn_3O_4 in the XRD spectrum because the content of Mn_3O_4 is relatively low and the dispersion degree is high.[30] Compared with the original CoS_2 and Mn_3O_4 diffraction peaks, the diffraction peak intensity of the composite catalysts decreased and the peaks were relatively broad, which indicated that CoS_2 was successfully introduced into the mixed photocatalyst.[31]

3.3. XPS

XPS is used to characterize the presence and chemical valence of elements in composite materials. As shown in **Figure 3**a, the full spectrum shows the presence of Mn, O, Co, and S elements in the 50 mg Mn_3O_4/CoS_2 composite. Figure 3b shows the XPS spectrum of Co 2p in 50 mg Mn_3O_4/CoS_2, which can be deconvoluted into six peaks with binding energies at 778.23, 780.90, 785.20, 793.56, 797.20, and 802.36 eV. Two apparent peaks at

778.23 and 793.56 eV are related to Co $2p_{3/2}$ and Co $2p_{1/2}$ from CoS_2, mainly in the form of Co^{2+}.[32,33] The binding energies at 780.9 and 797.2 eV are in accordance with Co $2p_{3/2}$ and Co$2p_{1/2}$ from Co—S, which may be due to the sample being easily accessible to air. In addition, two peaks locating at 785.2 and 802.3 eV are the satellite peaks of Co 2p.[34,35] Figure 3c shows that the XPS peaks of S 2p at 161.37 and 162.62 eV correspond to S $2p_{3/2}$ and S $2p_{1/2}$, respectively, confirming the presence of the predominant form of S^{2-} in the 50 mg Mn_3O_4/CoS_2 complex.[36] In addition, two peaks at 167.75 and 168.82 eV of S 2p correspond to sulfide oxide due to the sulfides being easily affected by contact with air.[37] The XPS spectrum of O 1s for the composite sample is shown in Figure 3d. Located at 529.8, 530.44, 531.18, and 532.14 eV are O 1s peaks, corresponding to Mn—O—Mn, lattice oxygen, surface hydroxyl, and absorbed oxygen.[38,39] In the XPS spectrum of Mn 2p (Figure 3e), it can be divided into two peaks. The peaks with binding energies of 641.36 and 652.93 eV were assigned to Mn $2p_{1/2}$ and Mn $2p_{3/2}$, respectively, and the difference in binding energy between the two was 11.57, which is consistent with the literature.[40] As the content of Mn_3O_4 in the composite catalyst is relatively small, the peak of Mn is relatively weak, and the result corresponds to the SEM characterization. All XPS results further confirmed the successful synthesis of the composite catalytic material Mn_3O_4/CoS_2.

3.4. Brunauer–Emmett–Teller (BET) Analysis

The BET value of photocatalytic materials was explored by nitrogen adsorption–desorption isotherms and pore size distribution, as shown in **Figure 4**. As Figure 4a, photocatalysts are shown as type IV adsorption and desorption curve.[41] At high relative pressure ($P/P_0 = 0.9$–1), the 50 mg Mn_3O_4/CoS_2 composite catalyst exhibited relatively high adsorption performance, revealing the existence of accumulated pore.[42] In Figure 4b, the pore size distribution shows that the photocatalyst mainly exists in the form of mesoporous structure (2–50 nm), and the pore size distribution is concentrated. The specific surface area and pore size of the catalysts are shown in **Table 1**. The measured specific surface areas of pure Mn_3O_4, pure CoS_2, and 50 mg Mn_3O_4/CoS_2 catalysts are 24.13, 9.81, and 22.68 $m^2 g^{-1}$, respectively. These parameters confirm that the introduction of CoS_2 has no obvious effect on the surface area of Mn_3O_4/CoS_2 nanocomposites. It is further indicated that the surface area may not be an important factor to enhance the hydrogen production performance of binary composites Mn_3O_4/CoS_2.[43] The average pore diameters of pure Mn_3O_4, pure CoS_2, and 50 mg Mn_3O_4/CoS_2 catalysts are 22.68, 26.43, and 33.74 nm, respectively. After introducing CoS_2, the composite catalysts show large pore diameters, which may be helpful to improve the hydrogen production performance. The composite catalyst 50 mg Mn_3O_4/CoS_2 has a larger pore volume and pore size than pure Mn_3O_4 and pure CoS_2. This is because the load of metallic sulfides facilitates electron transport.

3.5. Photocatalytic Hydrogen Evolution Activity Analysis

The photocatalytic H_2 production performance of the prepared material was studied. **Figure 5**a measured the photocatalytic hydrogen evolution amount of CoS_2 with different Mn_3O_4
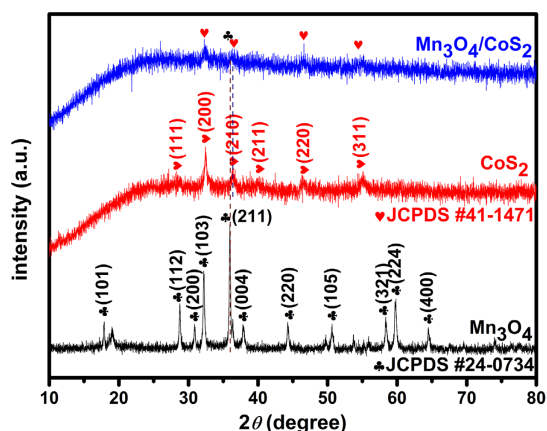

Figure 2. XRD patterns of Mn_3O_4, CoS_2, and 50 mg Mn_3O_4/CoS_2 materials.

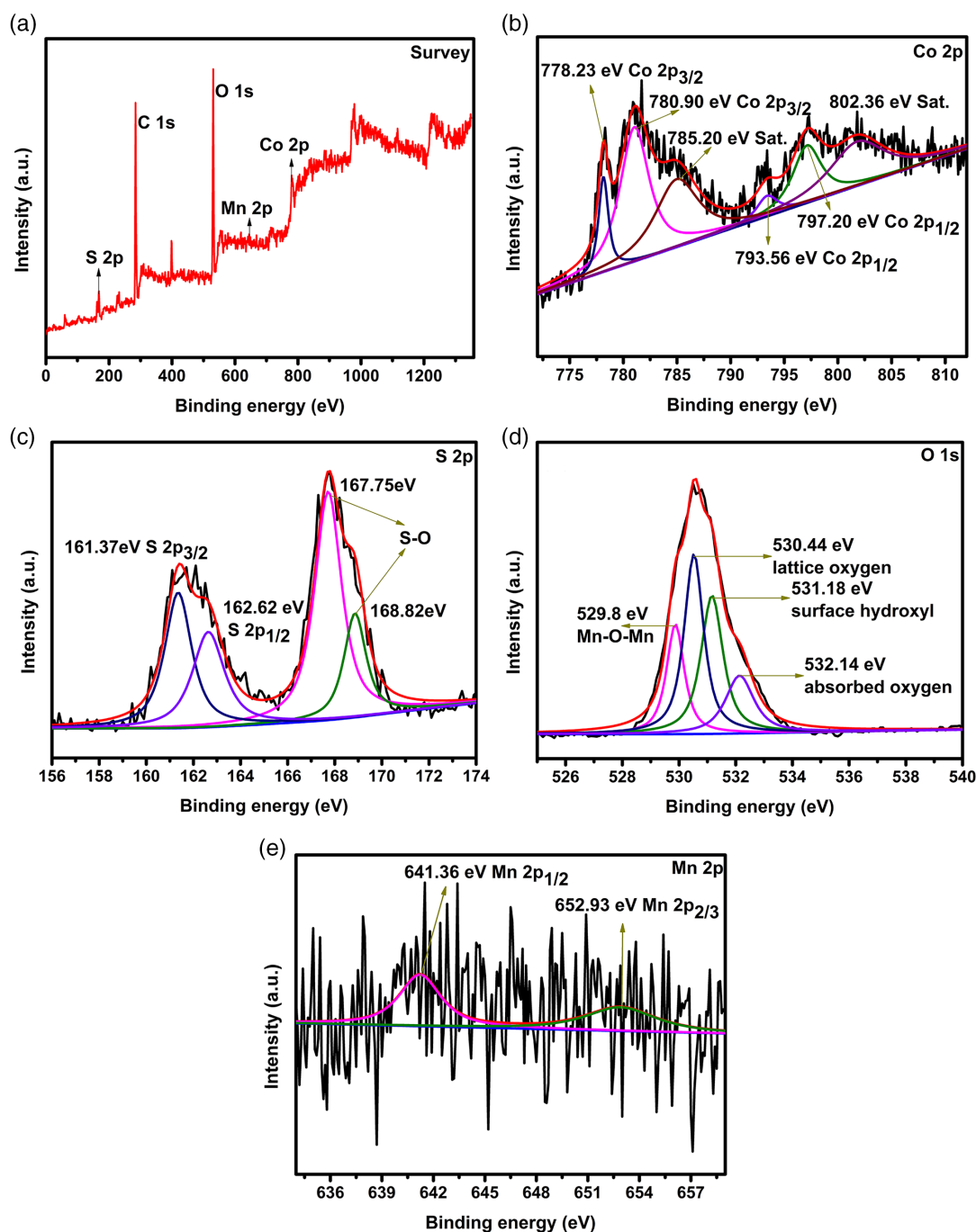**Figure 3.** XPS patterns of 50 mg Mn_3O_4/CoS_2 materials. a) Survey spectrum, b) Co 2p, c) S 2p, d) O 1s, and e) Mn 2p of 50 mg Mn_3O_4/CoS_2 composite.

contents. As shown in the figure, with the increase of Mn_3O_4 content from 10 to 50 mg, its hydrogen production activity increases obviously. When Mn_3O_4 is 50 mg, its hydrogen production reaches the maximum. When Mn_3O_4 is further increased, its hydrogen production activity decreases. The 50 mg Mn_3O_4/CoS_2 material has the highest H_2 production activity. A possible reason for this is that the best proportion of catalysts can expose more active sites.[44] However, excessive Mn_3O_4 may cover up the active site of the catalyst, restrict the absorption and utilization of

light, and thus reduce the amount of hydrogen evolution.[29] In Figure 5b, the photocatalytic hydrogen production amount of Mn_3O_4 and CoS_2 was 21.27 and 197.57 μmol in 5 h, respectively. It can be seen that 50 mg Mn_3O_4/CoS_2 enhanced the photocatalytic H_2 production performance of CoS_2. The hydrogen production of Mn_3O_4 was 318 μmol, which was ≈14.95 times higher than that of Mn_3O_4. For the EY-sensitized system, the EY content also plays a vital role on the photocatalytic hydrogen evolution. As the EY concentration increases, the hydrogen production amount
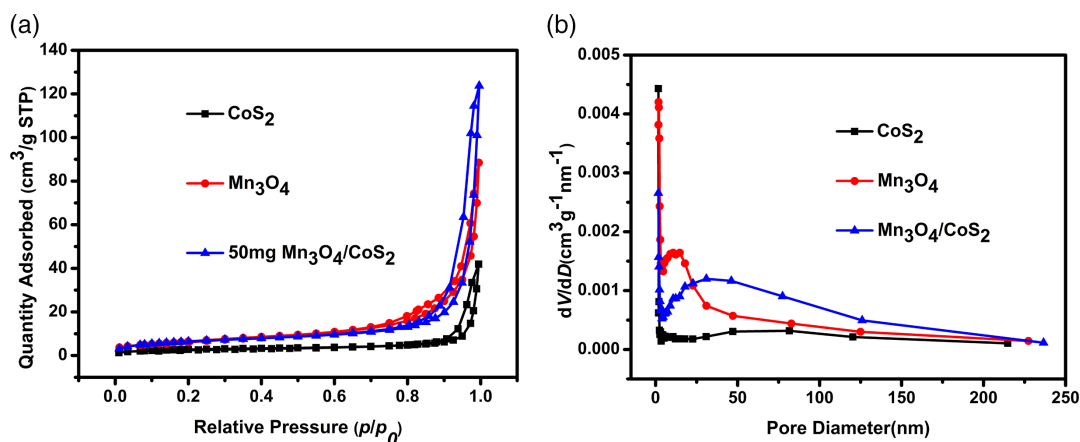
ADVANCED
SCIENCE NEWS
www.advancedsciencenews.com

physica
pss
status
solidi
a

www.pss-a.com

Figure 4. a) N_2 adsorption–desorption isotherms; b) pore size distribution plot of Mn_3O_4, CoS_2, and 50 mg Mn_3O_4/CoS_2 materials.

Table 1. Parameter obtained from physical adsorption instrument.

Sample	S_{BET} [$m^2 g^{-1}$]	Pore volume [$cm^3 g^{-1}$]	Average pore size [nm]
Mn_3O_4	24.13	0.14	22.68
CoS_2	9.81	0.07	26.43
50 mg Mn_3O_4/CoS_2	22.68	0.19	33.74

of the CoS_2/Mn_3O_4 sample increases (Figure 5c). When EY reaches 20 mg, the H_2 evolution amount of 50 mg CoS_2/Mn_3O_4 materials reaches the maximum value. The main reason is that the catalyst-adsorbed EY can absorb more photons and become the most significant active center. When continuing to increase the EY concentration, the H_2 production capacity decreases. The reason is that the absorbed EY is saturated. If
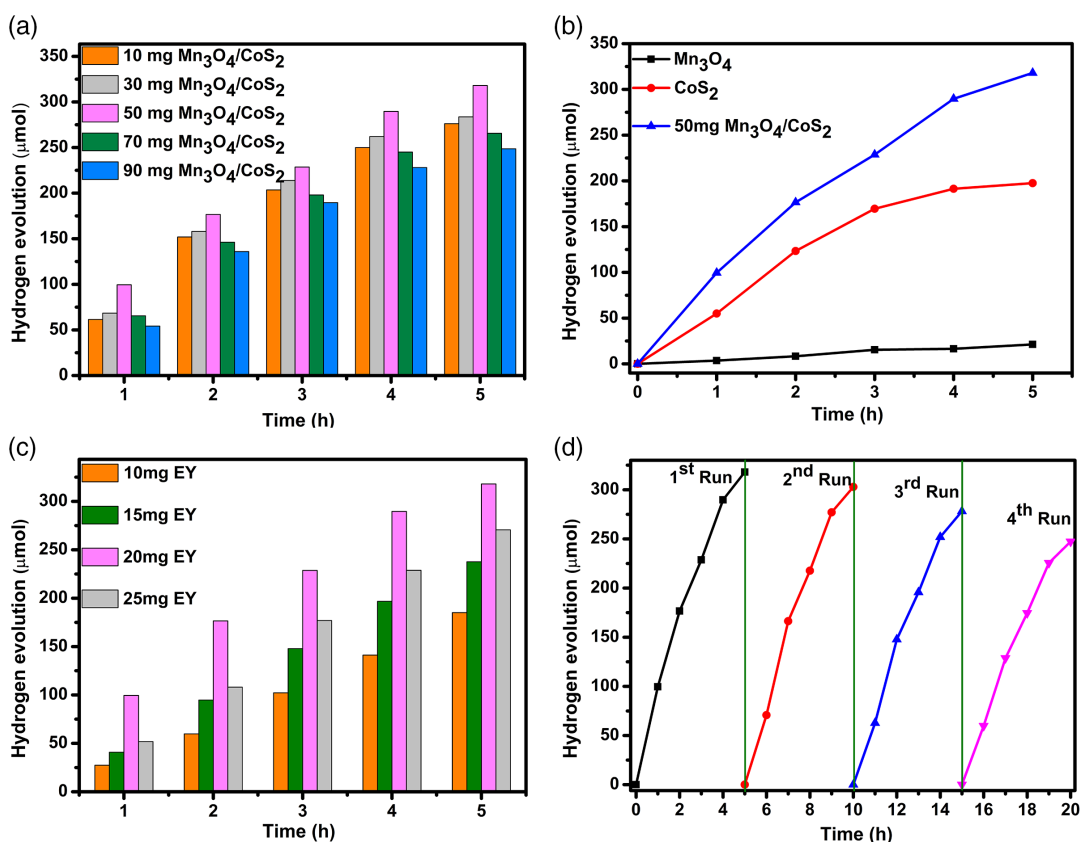

Figure 5. a) H_2 evolution amount of the different Mn_3O_4 in CoS_2 catalyst (TEOA, pH = 10); b) the H_2 evolution performance of Mn_3O_4, CoS_2, Mn_3O_4/CoS_2 samples; c) hydrogen production performance with different EY contents; and d) the photocatalytic stability for H_2 production of 50 mg Mn_3O_4/CoS_2 sample.

the EY content continues to increase, the high concentration (EY) will hinder the absorption of light, thus reducing the light utilization efficiency and significantly reducing the photocatalytic performance.[45] The photocatalytic stability of the 50 mg Mn_3O_4/CoS_2 photocatalyst was also studied. As shown in Figure 5d, the photocatalytic reaction was conducted for 20 h and detected intermittently every 5 h. During the third and fourth cycles, the hydrogen production of the composite catalyst decreased slightly, which may be due to the partial loss of the sample during centrifugation. The aforementioned results show that our photocatalyst 50 mg Mn_3O_4/CoS_2 has stable photocatalytic activity.

3.6. UV–Vis Diffuse Reflectance Spectra

Figure 6a shows the UV–vis diffuse reflectance spectra of the Mn_3O_4, CoS_2, and 50 mg Mn_3O_4/CoS_2. The absorption edge of Mn_3O_4 is around 620 nm. Pure Mn_3O_4 is unresponsive in the visible region. The response range of Mn_3O_4 in the visible-light region is expanded by combining with CoS_2. Strong light absorption could improve the hydrogen evolution activity of the catalyst, and the composite catalyst 50 mg Mn_3O_4/CoS_2 shows the strongest light absorption, which is consistent with the experiment results of hydrogen production. Figure 6b shows the bandgap values of Mn_3O_4, CoS_2, and 50 mg Mn_3O_4/CoS_2 calculated by the Kubelka–Munk function, which are 0.89, 0.75, and 0.55 eV, respectively. The bandgap of the composite catalyst 50 mg Mn_3O_4/CoS_2 is smaller than that of the pure Mn_3O_4 and pure CoS_2, which indicates that the composite catalyst 50 mg Mn_3O_4/CoS_2 is more conducive to electron transfer and thus improves the performance of photocatalytic hydrogen evolution.

3.7. Photoelectrochemical Measurement Analysis

To explore the transport and separation of charge carriers in samples, the time-varying photocurrent response (*it*) and linear sweep voltammetry (LSV) were measured. **Figure 7**a is the photocurrent response curve of the catalyst. It can be seen from it that the photocurrent response of the catalyst increases immediately and reaches a constant value when illuminated. When the illumination is stopped, the photocurrent intensity of the sample drops rapidly to zero. Under visible-light irradiation, the maximum photocurrent density of the 50 mg Mn_3O_4/CoS_2 composite catalyst electrode is $\approx 15\,\mu A\,cm^{-2}$; compared with the pure catalysts Mn_3O_4 and CoS_2, the photocurrent intensity of the composite catalyst is significantly enhanced. This indicates that the composite catalyst 50 mg Mn_3O_4/CoS_2 is more effective in improving the separation efficiency of charge carriers and is helpful in inhibiting the combination of photogenerated electrons and holes.[46]

In addition, the electrochemical hydrogen production activities of EY-sensitized Mn_3O_4, CoS_2 and 50 mg Mn_3O_4/CoS_2 were further studied by LSV. As shown in Figure 7b, there is a poor current response on the ITO electrode, whether at low or high potential. Mn_3O_4, CoS_2, and 50 mg Mn_3O_4/CoS_2 electrodes have little difference in current density and low current intensity in the range of 0.2 to -0.28 V potential, which is mainly due to the cathodic current generated when H^+ is reduced to H_2 (-0.5 to 0.6 V).[47] Subsequently, in the range -0.5 to -0.6 V voltage, it can be observed that the composite catalyst 50 mg Mn_3O_4/CoS_2 has the highest current density compared with pure Mn_3O_4 and pure CoS_2. This clearly shows that 50 mg Mn_3O_4/CoS_2 can effectively accelerate the migration of photogenerated electrons, and the composite can effectively improve the activity of hydrogen production.[48]

Electrochemical impedance spectroscopy (EIS) impedance maps of Mn_3O_4, CoS_2, and 50 mg Mn_3O_4/CoS_2, are shown in Figure 7c. The diameter of the semicircle in the curve reflects the impedance of the interfacial charge transfer. As shown in Figure 7c, the semicircle diameter of the sample CoS_2, Mn_3O_4, and 50 mg Mn_3O_4/CoS_2 decreases once. The results show that the interface resistance of the single CoS_2 electrode is the largest, which is not conducive to the efficient transfer of charge.[49–52] It can be observed that the order of resistance of electron transmission is $CoS_2 > Mn_3O_4 > 50$ mg Mn_3O_4/CoS_2, which demonstrates that the electrode impedance of 50 mg Mn_3O_4/CoS_2 is the smallest. And 50 mg Mn_3O_4/CoS_2 can improve the ability of internal charge separation and transfer.

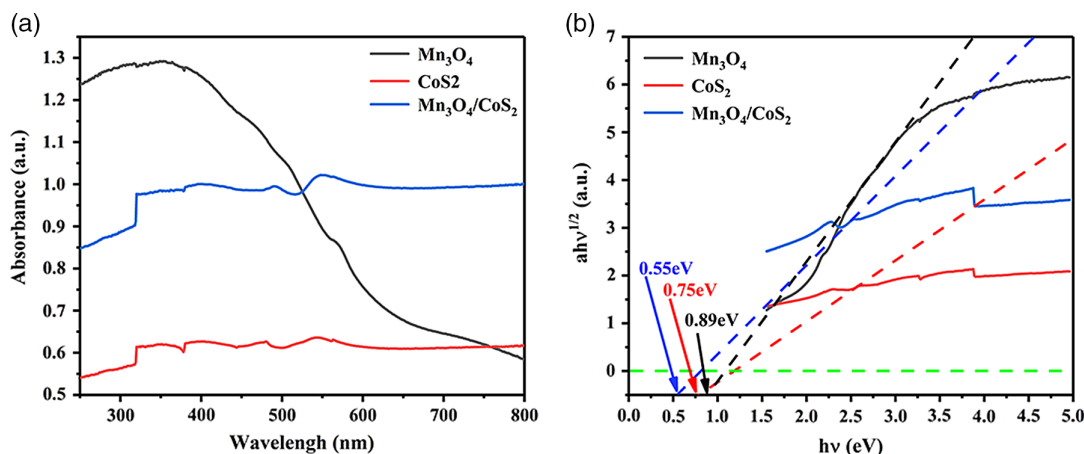**Figure 6.** a) The UV–vis DRS of Mn_3O_4, CoS_2, and 50 mg Mn_3O_4/CoS_2; b) the bandgap of Mn_3O_4, CoS_2, and 50 mg Mn_3O_4/CoS_2.
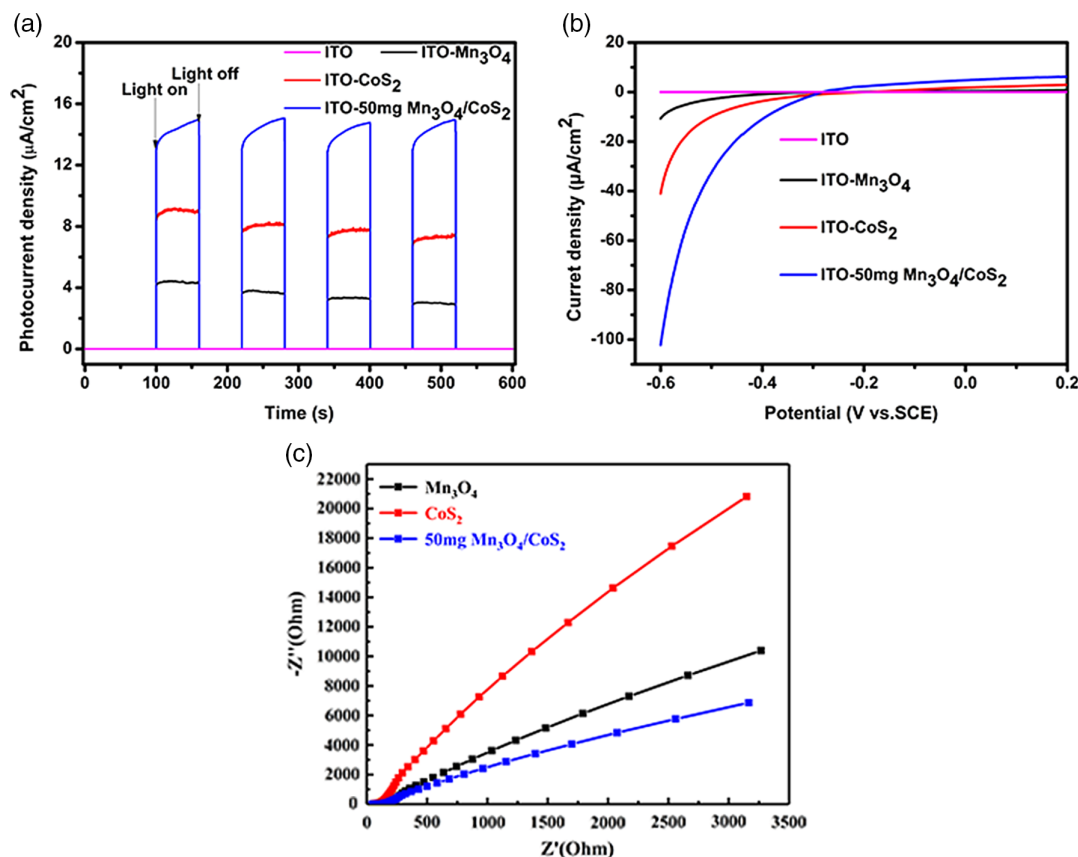
Figure 7. a) IT curves; b) LSV curves of Mn_3O_4, CoS_2, and 50 mg Mn_3O_4/CoS_2 samples in Na_2SO_4 (0.2 mol L^{-1}). The scan rate was 0.5 mV s^{-1}. c) EIS of Mn_3O_4, CoS_2, and 50 mg Mn_3O_4/CoS_2.

3.8. Photoluminescence Properties

Photoluminescence is a powerful characterization of photogenerated charge transfer. To understand the migration and separation of photogenerated carriers in samples, fluorescence studies of catalysts EY, EY-Mn_3O_4, EY-CoS_2, and EY-50 mg Mn_3O_4/CoS_2
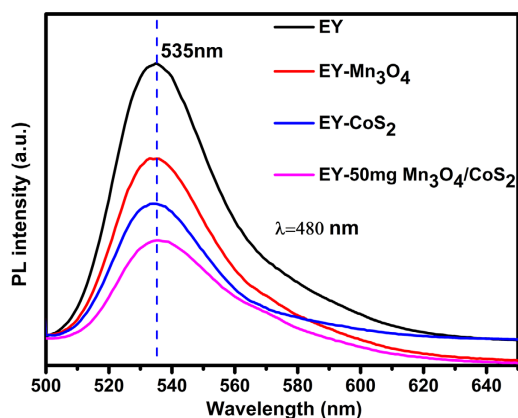

Figure 8. Steady-state PL spectra of the EY, EY-Mn_3O_4, EY-CoS_2, and EY-50 mg Mn_3O_4/CoS_2 system in TEOA aqueous solution (10%, pH = 10, EY = 1×10^{-6}).

were conducted at room temperature. **Figure 8**a shows PL spectra of EY, EY-Mn_3O_4, EY-CoS_2, and EY-50 mg Mn_3O_4/CoS_2 samples with excitation wavelength of 480 nm. The PL spectrum of pure EY has a strong emission peak centered at 535 nm, which indicates that photogenerated electrons and holes are easily recombined in EY.[53] Obviously, compared with pure EY, the PL emission intensity of EY-Mn_3O_4 and EY-CoS_2 decreases slightly, and the recombination rate of photogenerated electron holes decreases slightly. When both Mn_3O_4 and CoS_2 were added into EY, the fluorescence intensity decreased significantly and a slight redshift occurred. This phenomenon originates from the transfer of photogenerated electrons from Mn_3O_4 to the CoS_2 interface. The fluorescence quenching effect of the composite catalyst EY-50 mg Mn_3O_4/CoS_2 is the most significant. The results show that an effective electron transfer process is conducive to the separation of photogenerated electrons and holes, which plays a significant role in improving the photocatalytic performance.

3.9. Photocatalytic H_2 Evolution Schematic

According to the previous expression, the photocatalytic reaction process and the possibility principle of electron transfer in this article are shown in **Figure 9**. In Figure 9, EY is used as a
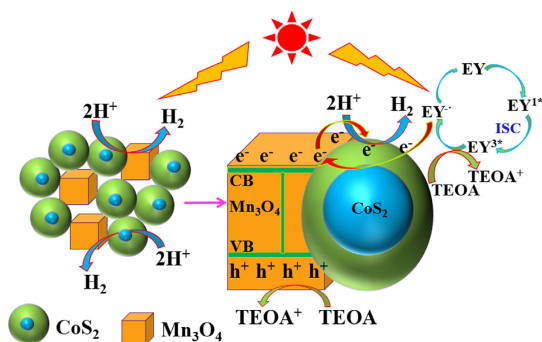
Figure 9. Photocatalytic mechanism for H_2 production in the EY-sensitized Mn_3O_4/CoS_2 system photocatalysts under visible-light irradiation.

In this study, a highly efficient and inexpensive composite photocatalyst was constructed by improving the transfer and separation of photogenerated electrons.

Conflict of Interest

The authors declare no conflict of interest.

Data Availability Statement

Research data are not shared.

sensitizer, TEOA is used as a sacrificial agent, and catalysts Mn_3O_4 and CoS_2 constitute heterojunction structures.

EY and Mn_3O_4, can be excited by light. The detailed steps are as follows:[54] 1) The EY molecule absorbs the photon energy and becomes a single excited state (EY^{1*}). Then, the singlet excited (EY^{1*}) state quickly turns to be the triplet excited state (EY^{3*}) by a valid intersystem crossing (ISC). The triplet excited state EY^{3*} is reduced to EY^- by the sacrificial agent TEOA and produces an oxidative electron donor ($TEOA^+$) at the same moment. Subsequently, a part of the electrons of $EY^-\cdot$ are transferred to the reaction site of CoS_2, at which time the protons are electron-reduced to obtain H_2. Another part of the electrons of EY^- is transferred to the conduction band (CB) of Mn_3O_4 and further transferred to CoS_2. Finally, the EY molecule returns to the ground state. 2) For Mn_3O_4, when the energy absorbed by Mn_3O_4 is greater than the forbidden bandgap, its electrons transition from the valence band (VB) to the CB, and Mn_3O_4 simultaneously leaves holes in the VB. These electrons are then further transferred to the reaction site of CoS_2. At this time, protons are reduced to obtain H_2, and holes of Mn_3O_4 in the VB are reduced by a sacrificial agent (TEOA).[55] In summary, this heterojunction structure promotes the efficient separation and transfer of photogenerated carriers, thereby improving the activity of photocatalytic H_2 production.

4. Conclusion

In summary, we have constructed a novel and easy-to-synthesize photocatalyst Mn_3O_4/CoS_2, and finally proposed a possibility of photocatalytic hydrogen production mechanism. The results show that the photocatalytic hydrogen evolution performance of the obtained Mn_3O_4/CoS_2 composites is significantly improved. By optimizing the addition amount of Mn_3O_4 and EY, the photocatalytic hydrogen evolution rate of Mn_3O_4/CoS_2 composite samples is 6360 $\mu mol\,g^{-1}\,h^{-1}$, and the hydrogen production is 14.95 times and 1.60 times that of Mn_3O_4 and CoS_2, respectively. Experimental characterization studies have shown the introduction of CoS_2 in the Mn_3O_4-supported catalyst promotes charge transfer and allows more electrons to be excited. The more effective photogenerated electrons are transferred to the active site of the photocatalyst. Therefore, the photocatalytic hydrogen evolution of the Mn_3O_4/CoS_2 composite is improved.

[1] X. Guo, X. Li, L. Qin, S.-Z. Kang, G. Li, *Appl. Catal., B* **2019**, *243*, 1.
[2] X. Han, D. Xu, L. An, C. Hou, Y. Li, Q. Zhang, H. Wang, *Appl. Catal., B* **2019**, *243*, 136.
[3] L. Miao, Q. Nie, J. Wang, G. Zhang, P. Zhang, *Appl. Catal., B* **2019**, *248*, 466.
[4] D. Xu, Y. Rui, V. T. Mbah, Y. Li, Q. Zhang, H. T. Wang, *Int. J. Hydrogen Energy* **2016**, *41*, 873.
[5] A. Belhadi, L. Boudjellal, S. Boumaza, M. Trari, *Int. J. Hydrogen Energy* **2018**, *43*, 3418.
[6] M. G. Joaquín-Morales, A. F. Fuentes, S. M. Montemayor, M. J. Meléndez-Zaragoza, J. S. Gutiérrez, A. López Ortiz, V. Collins-Martínez, *Int. J. Hydrogen Energy* **2019**, *44*, 12390.
[7] L. Wang, P. Wang, B. Huang, X. Ma, G. Wang, Y. Dai, X. Zhang, X. Qin, *Appl. Surf. Sci.* **2017**, *391*, 557.
[8] A. Kudo, *Pure Appl. Chem.* **2007**, *79*, 1917.
[9] M. Wiechen, M. M. Najafpour, S. I. Allakhverdiev, L. Spiccia, *Energy Environ. Sci.* **2014**, *7*, 2203.
[10] K. Govindan, H. T. Chandran, M. Raja, S. U. Maheswari, M. Rangarajan, *J. Photochem. Photobiol. A* **2017**, *341*, 146.
[11] A. J. Carrillo, D. P. Serrano, P. Pizarro, J. M. Coronado, *Energy Procedia* **2015**, *73*, 263.
[12] A. Gagrani, B. Ding, Y. Wang, T. Tsuzuki, *Mater. Chem. Phys.* **2019**, *231*, 41.
[13] Y. Tan, L. Meng, Q. Peng, Y. Li, *Chem. Commun.* **2011**, *47*, 1172.
[14] S. Xing, Z. Zhou, Z. Ma, Y. Wu, *Mater. Lett.* **2011**, *65*, 517.
[15] C. Ottone, M. Armandi, S. Hernández, S. Bensaid, M. Fontana, C. F. Pirri, G. Saracco, E. Garrone, B. Bonelli, *Chem. Eng. J.* **2015**, *278*, 36.
[16] Z. Zhao, J. Zhao, C. Yang, *Chem. Eng. J.* **2017**, *327*, 481.
[17] K. Li, C. Zhang, X. Li, Y. Du, P. Yang, M. Zhu, *Catal. Today* **2019**, *335*, 173.

[18] H. Ashassi-Sorkhabi, B. Rezaei-Moghadam, E. Asghari, R. Bagheri, Z. Hosseinpour, *Chem. Eng. J.* **2017**, *308*, 275.

[19] W. Chen, G.-B. Huang, H. Song, J. Zhang, *J. Mater. Chem. A* **2020**, *8*, 20963.

[20] J. Li, X. Liu, J. Zhang, *ChemSusChem* **2020**, *13*, 2996.

[21] J. Zhang, R. Cui, C. Gao, L. Bian, Y. Pu, X. Zhu, X. Li, W. Huang, *Small* **2019**, *15*, 1904688.

[22] P. Xu, W. Lu, J. Zhang, L. Zhang, *ACS Sustain. Chem. Eng* **2020**, *8*, 12366.

[23] Y. Cui, C. Zhou, X. Li, Y. Gao, J. Zhang, *Electrochim. Acta* **2017**, *228*, 428.

[24] Y.-R. Liu, X. Shang, W.-K. Gao, B. Dong, J.-Q. Chi, X. Li, K.-L. Yan, Y.-M. Chai, Y.-Q. Liu, C.-G. Liu, *Appl. Surf. Sci.* **2017**, *412*, 138.

[25] B. Ma, Y. Wang, X. Tong, X. Guo, Z. Zheng, X. Guo, *Catal. Sci. Technol.* **2017**, *7*, 2805.

[26] H. Wang, Y. Li, Y. Li, B. He, R. Wang, Y. Gong, *Int. J. Hydrogen Energy* **2018**, *43*, 23319.

[27] Y. Jing, X. Mu, C. Xie, H. Liu, R. Yan, H. Dai, C. Liu, X.-D. Zhang, *Int. J. Hydrogen Energy* **2019**, *44*, 809.

[28] Y.-R. Liu, W.-H. Hu, X. Li, B. Dong, X. Shang, G.-Q. Han, Y.-M. Chai, Y.-Q. Liu, C.-G. Liu, *Appl. Surf. Sci.* **2016**, *384*, 51.

[29] Y.-J. Yuan, Z. Li, S. Wu, D. Chen, L.-X. Yang, D. Cao, W.-G. Tu, Z.-T. Yu, Z.-G. Zou, *Chem. Eng. J.* **2018**, *350*, 335.

[30] Z. Qin, F. Xue, Y. Chen, S. Shen, L. Guo, *Appl. Catal., B* **2017**, *217*, 551.

[31] R.-B. Wei, Z.-L. Huang, G.-H. Gu, Z. Wang, L. Zeng, Y. Chen, Z.-Q. Liu, *Appl. Catal., B* **2018**, *231*, 101.

[32] J. Liu, D. Xue, *J. Cryst. Growth* **2009**, *311*, 500.

[33] X. X. Duan, Z. Gao, J. Chang, D. Wu, P. Ma, J. He, F. Xu, S. Gao, K. Jiang, *Electrochim. Acta* **2013**, *114*, 173.

[34] S. Peng, L. Li, X. Han, W. Sun, M. Srinivasan, S. G. Mhaisalkar, F. Cheng, Q. Yan, J. Chen, S. Ramakrishna, *Angew. Chem., Int. Ed.* **2015**, *126*, 12802.

[35] F. Li, J. Li, Z. Cao, X. Lin, X. Li, Y. Fang, X.. An, Y. Fu, J. Jin, R. Li, *J. Mater. Chem. A* **2015**, *3*, 21772.

[36] Z. Gao, N. Liu, D. Wu, W. Tao, F. Xu, K. Jiang, *Appl. Surf. Sci.* **2012**, *258*, 2473.

[37] Y. Yang, F. Li, W. Li, W. Gao, H. Wen, J. Li, Y. Hu, Y. Luo, R. Li, *Int. J. Hydrogen Energy* **2017**, *42*, 6665.

[38] F. Tian, A. M. Cerro, A. M. Mosier, H. K. Wayment-Steele, R. S. Shine, A. Park, E. R. Webster, L. E. Johnson, M. S. Johal, L. Benz, *J. Phys. Chem. C* **2014**, *118*, 14449.

[39] H. Cai, L. Sun, Y. Wang, T. Song, M. Bao, X. Yang, *Chem. Eng. J.* **2019**, *369*, 1078.

[40] A. Moses Ezhil Raj, S. G. Victoria, V. B. Jothy, C. Ravidhas, J. Wollschläger, M. Suendorf, M. Neumann, M. Jayachandran, C. Sanjeeviraja, *Appl. Surf. Sci.* **2010**, *256*, 2920.

[41] X. Zhang, Y. Guo, J. Tian, B. Sun, Z. Liang, X. Xu, H. Cui, *Appl. Catal., B* **2018**, *232*, 355.

[42] M.-h. Wu, L. Li, Y.-c. Xue, G. Xu, L. Tang, N. Liu, W.-y. Huang, *Appl. Catal., B* **2018**, *228*, 103.

[43] D. Jiang, B. Wen, Y. Zhang, Y. Jin, D. Li, M. Chen, *J. Colloid Interface Sci.* **2019**, *536*, 1.

[44] S. Song, J. Wang, T. Peng, W. Fu, L. Zan, *Appl. Catal., B* **2018**, *228*, 39.

[45] D. Liu, Z. Jin, Y. Bi, *Catal. Sci. Technol.* **2017**, *7*, 4478.

[46] X. Hu, S. Lu, J. Tian, N. Wei, X. Song, X. Wang, H. Cui, *Appl. Catal., B* **2019**, *241*, 329.

[47] Y. Li, Z. Jin, X. Hao, G. Wang, *Int. J. Hydrogen Energy* **2019**, *44*, 17909.

[48] X. Hao, Z. Jin, H. Yang, G. Lu, Y. Bi, *Appl. Catal., B* **2017**, *210*, 45.

[49] X. Hao, Z. Cui, J. Zhou, Y. Wang, Y. Hu, Y. Wang, Z. Zou, *Nano Energy* **2018**, *52*, 105.

[50] M. Ibrahim, K. Kannan, H. Parangusan, S. Eldeib, O. Shehata, M. Ismail, R. Zarandah, K. K. Sadasivuni, *Coatings* **2018**, *10*, 783.

[51] K. Kannan, M. H. Sliem, A. M. Abdullah, K. K. Sadasivuni, B. Kumar, *Catalysts* **2020**, *10*, 549.

[52] K. Kannan, K. K. Sadasivuni, A. M. Abdullah, B. Kumar, *Rev. Catal.* **2020**, *10*, 495.

[53] D. A. Reddy, E. H. Kim, M. Gopannagari, Y. Kim, D. P. Kumar, T. K. Kim, *Appl. Catal., B* **2019**, *241*, 491.

[54] Y. Zhang, Z. Jin, *Catal. Lett.* **2019**, *149*, 34.

[55] S. Min, Y. Lei, H. Sun, J. Hou, F. Wang, E. Cui, S. She, Z. Jin, J. Xu, X. Ma, *Mol. Catal.* **2017**, *440*, 190.